

Optimization of Water Based Drilling Fluid Properties with the SiO₂/g-C₃N₄ Hybrid

Anwar Ahmed, Erum Pervaiz,* Uzair Abdullah, and Tayyaba Noor

Cite This: *ACS Omega* 2024, 9, 15052–15064

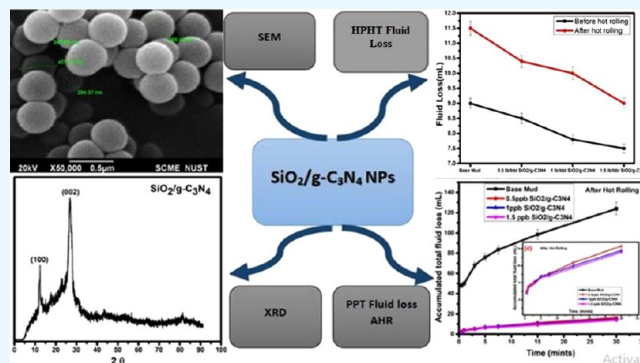
Read Online

ACCESS |

Metrics & More

Article Recommendations

ABSTRACT: Drilling fluids are an essential component of drilling operations in the oil and gas industry. Nanotechnology is being used to develop advanced drilling fluid additives. This study looked at the viability of synthesizing SiO₂/g-C₃N₄ hybrid extending the Stober process followed by its addition in different concentrations to water-based drilling fluids and studying impact on the rheological and fluid loss properties of the fluids. The synthesized hybrid was analyzed using XRD, SEM, TGA, and FTIR. Subsequently, it was used to develop the water-based drilling mud formulations and subjected to measurements in accordance with API standard practices. The studies were carried out at various SiO₂/g-C₃N₄ nanoparticle concentrations under before hot rolling (BHR) and after hot rolling (AHR) conditions. The outcomes demonstrated that the rheological and fluid loss properties were enhanced by the addition of SiO₂/g-C₃N₄ nanoparticles, as it worked in synergy with other additives. Additionally, it was discovered that the nanoparticles improved the drilling fluid thermal stability. The experimental findings indicate a significant influence of SiO₂/g-C₃N₄ nanoparticles on base fluid properties including rheology and fluid loss as the most remarkable, especially at higher temperatures. The significant improvements in yield point and 10 s gel strength were 55 and 42.8% under BHR and 216 and 140% under AHR conditions, respectively. Permeability plugging test (PPT) fluid loss was reduced by 69.6 and 87.2% under BHR and AHR conditions, respectively, when 0.5 lb/bbl nanoparticles were used in formulations. As a result, SiO₂/g-C₃N₄ nanomaterial has the potential to be used as drilling fluid additive in water-based drilling fluids.



1. INTRODUCTION

Drilling fluids are used in oil and gas and geothermal energy drilling operations to perform a variety of tasks, including removing drill cuttings, cooling and lubricating the drill bit, and supplying hydrostatic pressure to ensure borehole stability. The execution of these tasks depends on the lithology being drilled and a number of drilling fluid parameters that need to be optimized to achieve desired performance water base muds (WBM) have had various additives added to them to enhance performance.^{1,2} These materials, which include natural polymers like xanthan gum, are employed to develop rheological and filtration properties and to reduce wellbore instability issues.^{3–5} The thermal stability of these polymers becomes a noteworthy concern, as well as a technical and economic concern, as the well depth and bottom hole temperatures rise. Furthermore, it has been suggested that dispersing nanoparticles into drilling mud might enhance its performance, particularly in downhole circumstances.^{6–9} Therefore, further technological developments are required to address the high-pressure and high-temperature (HPHT) issues and minimize drilling problems.¹⁰ High thermal stability is needed for improved drilling mud systems to function in

HPHT environments and prevent mud deterioration. The downhole equipment, casing, and cement sheaths might be destroyed by these harsh circumstances.¹¹

Due to its hydrophilic characteristics, hydrophilic shale readily interacts with drilling fluid to become hydrated. It has been demonstrated that altering rock wettability can enhance wellbore stability.^{12,13} Small size, high surface reactivity, high adsorption capacity, and high specific surface area are characteristics of nanoparticles.¹⁴ According to reports, nanoparticles can enhance the rheology, lubricity, and inhibition of drilling fluids. Furthermore, it has been demonstrated that by actively blocking the pores in the shale, nanoparticles may stabilize the shale by lowering filtrate infiltration.^{15,16} The use of nanoparticles to change the wettability of rocks has also

Received: November 19, 2023

Revised: February 27, 2024

Accepted: March 4, 2024

Published: March 20, 2024



been the subject of several investigations.¹⁷ The research that has already been done on using nanoparticles to change rock wettability, however, has mostly been concerned with improving oil recovery.¹⁸

There are two approaches to manufacture hydrophobic surfaces: either by adding a nanoscale rough structure to a low surface energy surface or by chemically changing the rough surface. In this research, hydrophobically modified nanoparticles were created by treating low-surface-energy silica nanoparticles.¹² By changing the wellbore rock from hydrophilic to hydrophobic and using nanoparticles as plugs, the physicochemical interaction of the rock with water was hindered. They showed that nanoparticles worked well to block pore throats, greatly lowering the permeability of the shale in the process. Additionally, nanoparticles alone cannot seal the microcracks in shale, but when combined with other elements in drilling fluid, they had a positive synergistic impact.¹⁹ The previously reported silica nanoparticles may raise the yield point (YP) and plastic viscosity (PV) of WBDF and OBDF. The pH of nano WBDFs may decrease as a result of the interaction between the nanoparticles and hydroxyl ions. By physically sealing the wellbore and by the use of nanomaterials, such as silica nanoparticles, the potential of shale swelling and instability problems is greatly reduced. Higher quantities of SiO₂ NPs can result in better plugging effects.²⁰

The combination of smart polymers and nanosilica is an effective method for preventing free water intrusion into shale micronanopores during drilling and therefore assuring wellbore stability. Nano-SiO₂ has a strong potential for increasing the performance of low water-in-oil drilling fluids and high thermal stability with a decomposition temperature of 370 °C.^{21–23} Another research demonstrates that the use of hybrid silicate, both organic and inorganic, as a film-forming agent significantly improved well stability in water-based drilling fluids.²⁴ Another study revealed that silica NPs significantly improved shale inhibition with 96% shale recovery after hot rolling.^{25,26} In comparison to their bulk form, the carbon-based nanostructures exhibit exceptional chemical, mechanical, physical, and electrical properties.^{27,28} The carbon nanoparticles (CNPs) are being addressed to solve the technological and environmental difficulties associated with drilling. The rheology, shale inhibition, lubrication, and fluid loss control are all significantly improved by the use of carbon nanoparticles (CNPs), such as g-C₃N₄.^{29,30} This previous study provides in-depth information about the application of several CNPs to enhance the characteristics of drilling fluids. Carbon is widely regarded as the most versatile material ever invented, having the capacity to react with other compounds and produce a broad range of structural forms, resulting in significant industrial advances.^{31,32} The intention is to employ graphitic carbon nitrides, which have a huge surface area and improved thermal and mechanical qualities due to their 2D sheet structure.³³

The effects of different SiO₂/g-C₃N₄ concentrations on the rheology and filtration control performance of WBDF under HPHT conditions were examined in this work. Surface morphology, functional groups, particle structures, and rigidity of various SiO₂/g-C₃N₄ species have all had an impact on their surface characteristics and fluid interactions. As a result, in this work, SiO₂/g-C₃N₄ was synthesized by using a Stober approach using TEOS as the source of SiO₂ and melamine as the source of g-C₃N₄. Considering that g-C₃N₄ may improve

dispersion stability under high-temperature conditions, the possibility of employing these SiO₂/g-C₃N₄ to improve the filtration control capacity of water-based drilling fluids in severe high-temperature environments was explored. To the best of our knowledge, the use of SiO₂/g-C₃N₄ in drilling fluids has not been examined. Hence, this is an innovative work and would help in safe drilling of horizontal and extended reach wells to tap unconventional shale and tight sandstone reservoirs. Previously, attempts were made to improve fluid properties using graphite, which is pure carbon. However, using g-C₃N₄ instead of graphite is a step forward toward greener approach as it reduces the carbon footprint by replacing some carbon with nitrogen.

2. MATERIALS AND METHOD

For the synthesis of SiO₂/g-C₃N₄, the ingredients tetraethyl orthosilicate (TEOS), ammonia solution (NH₃), ethanol, deionized water, and melamine were acquired from Sigma-Aldrich and were of analytical grade.

The base fluids have been designed for optimum rheology and fluid loss characteristics. The base fluids contained soda ash (hardness controller), API bentonite (viscosity agent), NaOH (alkalinity source), KCl (shale inhibitor), polyanionic cellulose low viscosity (fluid loss controller), xanthan gum, modified starch, CaCO₃, and API barite.

2.1. Synthesis of Bare g-C₃N₄. The bulk of g-C₃N₄ was made using a procedure that has been documented in the literature.³⁴ Alumina crucible containing 20 g of melamine was placed in a muffle furnace and heated to 550 °C at a rate of 10 °C/min for 4 h. After that, the solution was kept at room temperature at 25 °C. A yellow cluster was produced after calcination; this cluster was then ground into a fine powder in a mortar and pestle.

2.2. Synthesis of SiO₂/g-C₃N₄ Hybrid Nanomaterial. Although the literature implies that the Stober synthesis can take many different forms,³⁵ the authors of this study opted to adopt the formulation described by Sivolapov et al.³⁶ As a result, 5 mL of TEOS, 6 mL of ammonia, 2 mL of deionized water, and 100 mL of a solvent (ethanol) were added to the reaction medium, which already included the presynthesized g-C₃N₄ powder. The aforementioned ingredients were mixed together on a magnetic stirrer for 5 h at 35 °C. The reaction was then continued under the same conditions for an additional 2 h after an additional 1 mL of TEOS was added. In order to boost the reaction's yield, more TEOS was added.³⁷ Studies show that adding TEOS once will result in fewer SiO₂ particles being produced, regardless of the amount added, than adding TEOS again to the reaction mixture. Additionally, larger sized NPs are produced as a result of this process, but their shape and size distribution are left unchanged. After the reaction, the system was repeatedly rinsed many times with deionized water, and the residual solvents were then removed using a rotary centrifuge.

2.3. Characterizations. The crystallinity and compositional analyses of the hybrids as-fabricated were assessed by X-ray diffraction (XRD) (STOE-SEIFERTX'PER PRO), with values of 2θ ranging from 0 to 90° using Cu–K radiation. Using energy-dispersive X-ray microscopy (EDX) and scanning electron microscopy (SEM) (JEOL-JSM-6490A), the surface morphology and structure of the prepared nanomaterial were examined. To determine the functional group of the nanomaterial, Fourier transform infrared spec-

Table 1. Chemicals Used in Synthesis of Water-Based Drilling Fluids

sr. no.	component	function	specific gravity	concentration (g/350 mL)	equivalent volume (mL)
1	deionized water	base fluid	1.00	318.59	318.59
2	soda ash	hardness controller	2.53	0.10	0.04
3	API bentonite	viscosity enhancer	2.60	5.00	1.92
4	sodium hydroxide	alkalinity source	2.10	0.20	0.10
5	potassium chloride	shale inhibitor	1.99	10.00	5.03
6	polyanionic cellulose low viscosity	fluid loss controller	1.50	2.00	1.33
7	xanthan gum	rheology modifier	1.50	1.00	0.67
8	modified starch	fluid loss controller	1.50	2.00	1.33
9	CaCO ₃ –5 micrometers	bridging material	2.70	5.00	1.85
10	CaCO ₃ –50 micrometers	bridging material	2.70	5.00	1.85
11	API barite	weighing agent	4.20	69.00	16.43

trospectroscopy (FTIR) methods are employed to obtain the infrared absorption spectra of powdered materials.

2.4. Preparation of SiO₂/g-C₃N₄ Nanofluids. Before being introduced to the base drilling fluid, the SiO₂/g-C₃N₄ nanoparticles were dispersed in 50 mL of deionized water and stirred at 600 rpm for 30 min to achieve a homogeneous solution. Thirty min of ultrasonication and dispersion were used to make the solutions homogeneous (Ultrasonic bath FB15051, Fisher brand).

2.5. Preparation of Water-Based Drilling Fluids Containing Nanoparticles. The formulated water-based drilling fluid system includes a number of the drilling fluid chemicals as listed in Table 1. The purpose of using all components is to develop a drilling fluid with good fluidity characteristics including rheology and fluid loss so as to evaluate the real effects of nanomaterials on these characteristics of drilling fluids under before and after hot rolling conditions. We employed the same formulation with 0.5, 1, and 1.5 g of nanomaterials per lab barrel of fluid (350 mL) to compare the results. Before each experiment, 50 mL of 0.5, 1, and 1.5 g of SiO₂/g-C₃N₄ nanofluids were introduced to the WBDF and continued mixing using a Hamilton beach mixer for 30 min developing material balanced formulations.

2.6. Drilling Fluid Properties Measurements.
2.6.1. Rheology Properties. Drilling fluid samples' rheological characteristics were assessed in accordance with the API's suggested methodology.³⁸ Briefly, the plastic viscosity (PV), yield point (YP), 10 s and 10 min gel strengths, as well as apparent viscosity (AV), were measured using a rotating viscometer, the Fann 35, which has six speeds of shear rate (3, 6, 100, 200, 300, and 600 rpm). PV is a measure of a fluid's resistance to flow; it is equivalent to the viscosity of mud caused by frictions between its solid particles. YP, on the other hand, refers to the initial stress needed to move the fluid. The results of the PV, YP, and AV calculations are shown below.

$$\text{apparent viscosity (AV)} = \phi_{600} / 2cP \quad (1)$$

$$\text{plastic viscosity (PV)} = \phi_{600} - \phi_{300}cP \quad (2)$$

$$\text{yield point (YP)} = (\phi_{300} - PV)lb / 100ft^2 \quad (3)$$

The units of AV and PV are cP, whereas YP was measured in lb/100 ft².

2.6.2. Filtration Properties. Using an API filter press (OFITE), the filtration rate of the drilling fluid was measured. The fluid was subjected to an applied pressure of 100 psi, which forced the filtrate to drain from it. Thirty minutes were

spent doing this at room temperature (25 °C) before the volume of fluid loss was measured.

2.6.3. High-Pressure and High-Temperature Filter Press (HPHT). An API high pressure and high temperature (HPHT) filter press was used in a stainless-steel filtration cell for static filtration testing. The measurements were made at a differential pressure of 500 psi and a temperature of 225 °F. The filtrate for filtration at 225 °F was collected by using a condenser.

2.6.4. Permeability Plugging Tester (PPT). Using a certified permeability plugging tester (PPT), the plugging effectiveness of the SiO₂/g-C₃N₄ was assessed using a 40 μm ceramic disc. The disc had a 3.5 in² filtration area that had been manufactured artificially. The PPT's schematic with the ceramic disc is shown in Figure 8a,b. Before being heated to the desired temperature (°F), the fluid is placed inside the PPT cell and pressured there at 1000 psi differential pressure. Controlling the top valve on the PPT cell induced flow when the sample was conditioned. The progression of filtration over time and at various pressures was observed.

3. RESULTS AND DISCUSSION

3.1. Powder X-ray Diffraction. The produced SiO₂/g-C₃N₄ hybrid powder X-ray diffraction pattern is shown in Figure 1. The XRD profiles for the SiO₂ nanospheres sample exhibit only strong and wide peaks in the 2θ = 15–35° range, which is attributed to amorphous SiO₂.³⁹ The amorphous nature of the deposited film is shown by the absence of a

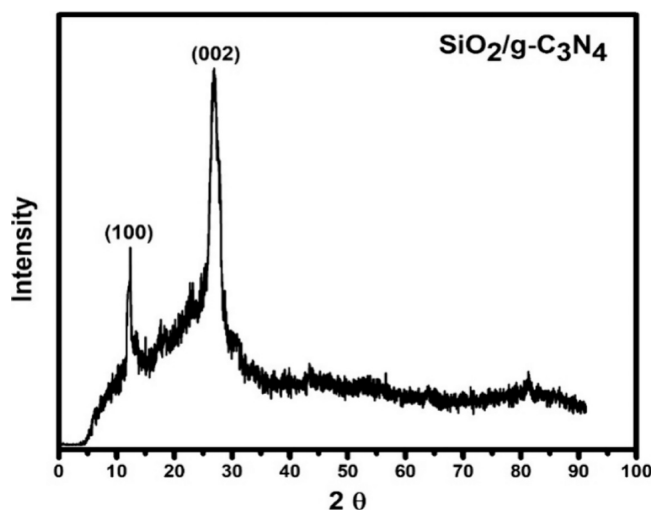


Figure 1. Powder X-ray diffraction of SiO₂/g-C₃N₄.

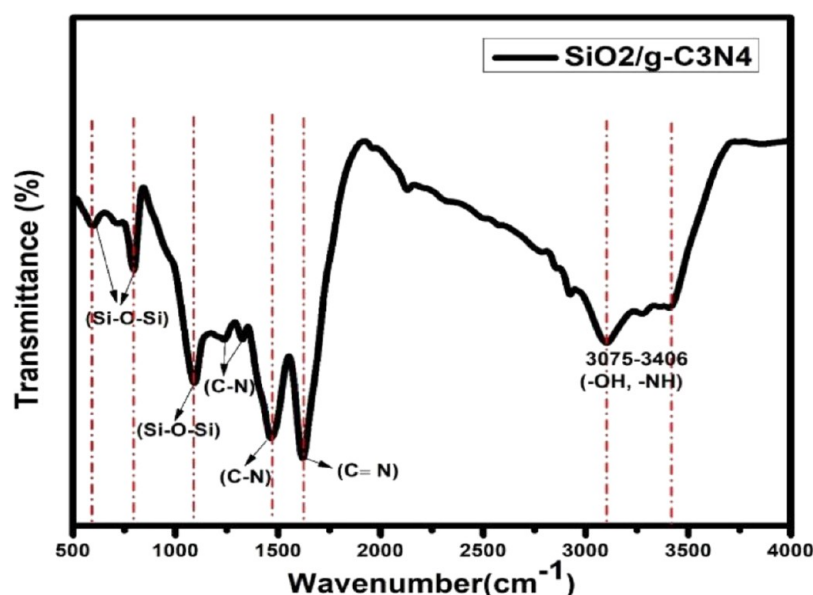


Figure 2. FTIR spectra of $\text{SiO}_2/\text{g-C}_3\text{N}_4$.

distinctive peak in the SiO_2 layer's XRD pattern.⁴⁰ There are two distinct diffraction peaks on it. The interlayer stacking of conjugated aromatic planes, indexed as (002), is assigned to the strong peak at 27° . Furthermore, the small peak at almost 12.5° is in plane indexed as (100) structural packing motif of tri-*s*-triazine units.^{41,42}

3.2. Fourier Transform Infrared spectroscopy (FTIR). The functional groups of $\text{SiO}_2/\text{g-C}_3\text{N}_4$ identified using FT-IR spectroscopy are shown in Figure 2. The spectral profile of the synthesized sample had prominent bands between 1100 and 1750 cm^{-1} . The aromatic C–N stretching vibrations were represented by the prominent peaks seen at about 1250, 1320, and 1460 cm^{-1} , whereas the C=N stretching vibrations could be found at 1569 cm^{-1} .^{43–46} The stretching vibrations of the hydroxyl groups (O–H) are at 3075 cm^{-1} and N–H at 3406 cm^{-1} . The distinctive adsorption maxima at 1090, 790, and 465 cm^{-1} are attributed to the bending vibration, asymmetric stretching, and symmetric stretching of Si–O–Si, respectively.^{47,48} The validity status of the silica particles was verified through examination of the amorphous structure, and the area of the wavelength number intrinsic to silica particles in the findings. Since no additional areas were found, it is believed that silica particles formed in this intrinsic region of wavenumber, which is the usual peak region of SiO_2 .⁴⁸

3.3. Microstructural and Elemental Composition Analysis. The $\text{SiO}_2/\text{g-C}_3\text{N}_4$ nanoparticles' surface morphology, size, and shape were examined using scanning electron microscopy (SEM). The spherical form of nanoparticles and the size of silica particles are both shown in the SEM image of SiO_2 . The produced nanoparticles for the whole SiO_2 concentration are clearly seen in Figure 3 to have a spherical shape with clearly defined borders and a particle size of 200–450 nm. Energy dispersive spectroscopy (EDS), stimulated with an electron beam (20 keV), was used to examine the elemental compositions of nanoparticles. Carbon (C) and oxygen (O) have peaks at 0.4 and 0.5 keV, respectively. While Si is responsible for the higher peak at 1.7 keV, Si and O are present in the investigated samples as the main elements, according to the EDS analysis.

In the hybrid sample, $\text{g-C}_3\text{N}_4$ exhibits a characteristic lamellar structure, which is produced by the aggregation of massive $\text{g-C}_3\text{N}_4$ particles. The representative SEM pictures of the $\text{SiO}_2/\text{g-C}_3\text{N}_4$ nanospheres are shown in Figure 3e. It can be seen that the structural characteristics of all of the $\text{SiO}_2/\text{g-C}_3\text{N}_4$ compounds are comparable. To obtain a typical $\text{SiO}_2/\text{g-C}_3\text{N}_4$ nanosphere, some of the SiO_2 nanoparticles uniformly distributed on the surface of 2D $\text{g-C}_3\text{N}_4$. All elements were observed to be distributed uniformly throughout the selected region as shown in EDS result Figure 3f. This suggests that the distribution of SiO_2 and $\text{g-C}_3\text{N}_4$ is uniform.

3.4. Thermogravimetric Analysis (TGA). The study of the $\text{SiO}_2/\text{g-C}_3\text{N}_4$ Nano hybrid by TGA is shown in Figure 4. Compared to pure $\text{g-C}_3\text{N}_4$, the $\text{SiO}_2/\text{g-C}_3\text{N}_4$ nanohybrid exhibits exceptional thermal stability. Below 120°C , both adsorbed and chemisorbed water evaporation takes place as shown in Figure up to 450°C , relatively stable oxygen-containing groups start to disintegrate, and they roughly start to become stable about 710°C . This demonstrates that below 500°C , the chemical characteristics of $\text{g-C}_3\text{N}_4$ are stable. The internal structure, which consists of an aromatic ring conjugated system coupled by a covalent connection between carbon and nitrogen, is the cause of this. However, $\text{g-C}_3\text{N}_4$ has a layered structure that resembles that of graphite. Between layers, there is a rather strong van der Waals force.⁴⁹ As the temperature increases from the initial 500°C point, $\text{g-C}_3\text{N}_4$ begins to disintegrate. At 710°C , $\text{g-C}_3\text{N}_4$ totally disintegrates. The mass of $\text{g-C}_3\text{N}_4$ is 0 at this moment. This is consistent with where the curve's inflection point is located. Below 900°C , SiO_2 essentially has no mass loss. Below 900°C , it has high thermochemical stability.⁵⁰ The fraction of SiO_2 in the sample may be calculated using the value of the curve's inflection point and the features of $\text{g-C}_3\text{N}_4$ and SiO_2 in the TG curve. The amount of SiO_2 in $\text{SiO}_2/\text{g-C}_3\text{N}_4$ is 20% and nano- SiO_2 has excellent thermal properties.

3.5. Effect of Synthesized Nanomaterial on the Established Drilling Fluid System's Filtration and Rheological Properties. The rheological properties of the drilling fluids are important characteristics that affect several essential aspects of the drilling operation. The fluid's yield

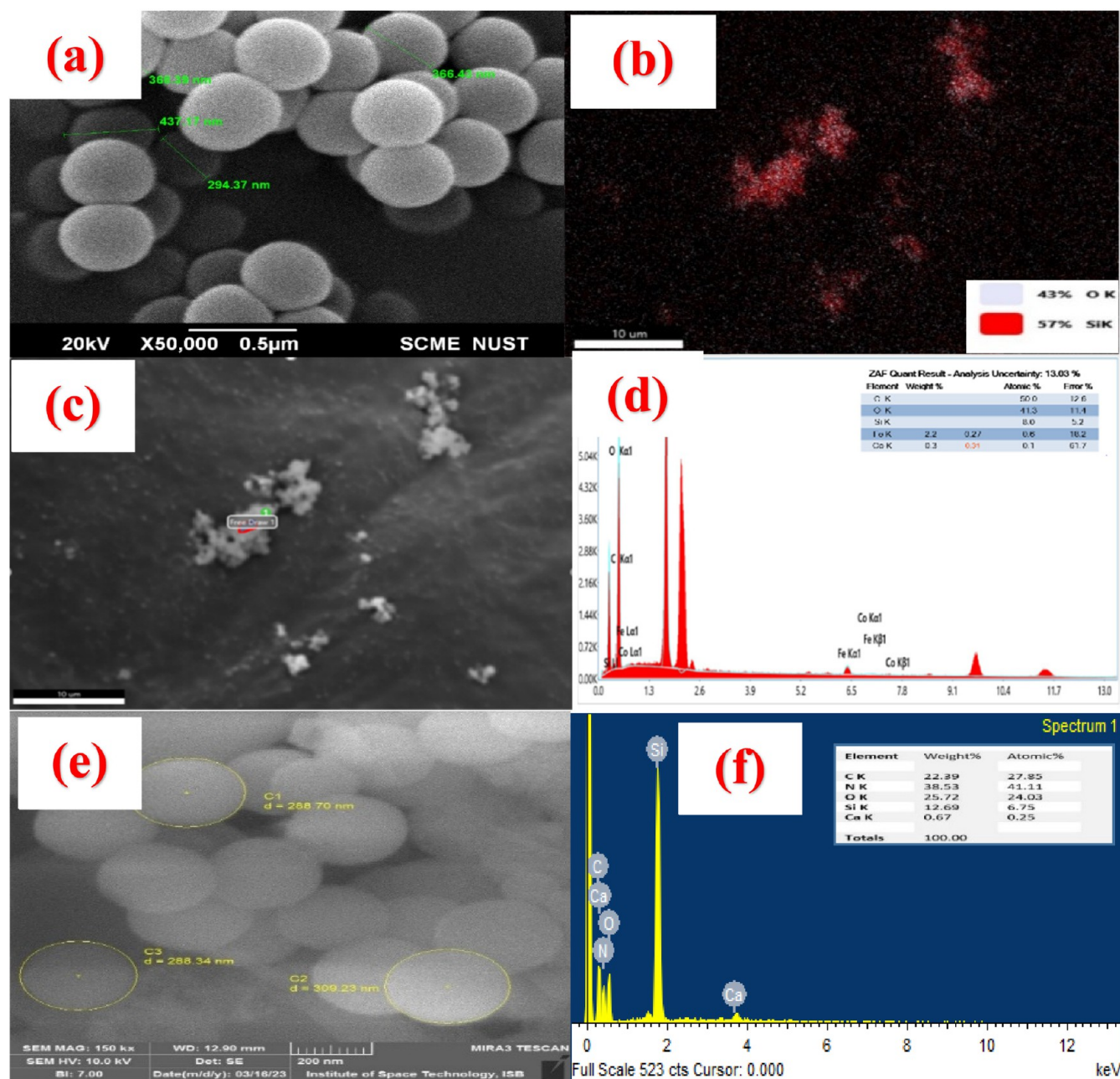


Figure 3. (a) SEM image of bare SiO₂. (b) Corresponding element mapping of bare SiO₂. (c) Area selection for EDS. (d) Elemental composition EDS. (e) SEM image of SiO₂/g-C₃N₄. (f) Corresponding elemental composition of the hybrid sample.

point, apparent viscosity, plastic viscosity, and gelling characteristics are its most important rheological characteristics. These rheological properties are successfully attained in drilling fluids based on nanocomposite materials. The fundamental rheological properties of the manufactured muds were evaluated including plastic viscosity, yield point, gel strength, filter cake thickness, and filtrate loss. The parameters for plastic viscosity and yield point as well as mud viscosity and gel strength were determined using a Fann viscometer (model 35SA). The sample was first heated to 120 °F in a Thermo-cup. The Fann viscometer speed was then set to 600 and 300 rpm to calculate the values of the plastic viscosity and yield point at each speed. Furthermore, the filter cake and filter loss were evaluated with an OFITE filter press (141-00-C). The filter press includes a pressured chamber

with filter media fitted. Figure 6 depicts the configuration for the OFITE filter press. In order to increase the cell pressure to 100 psi, a CO₂ cartridge was attached to the filter press apparatus. In the cell, the prepared mud was loaded to within a quarter in. of the O-ring groove. To determine the filtrate value, a suitably graduated cylinder was positioned beneath the filtrate aperture. The cell's pressure-applying intake valve was then opened. Every test took place over a period of 30 min. The cell was disassembled, and the mud was discarded after diluting with water. It should be emphasized that the dismantling must be done slowly and carefully to avoid disturbing or harming the mud cake that has been developed. The cake was then properly cleaned to remove the extra mud. After then, the thickness of the mud cake was determined. Table 2 and Figure 5 illustrate the impact of nanocomposite on

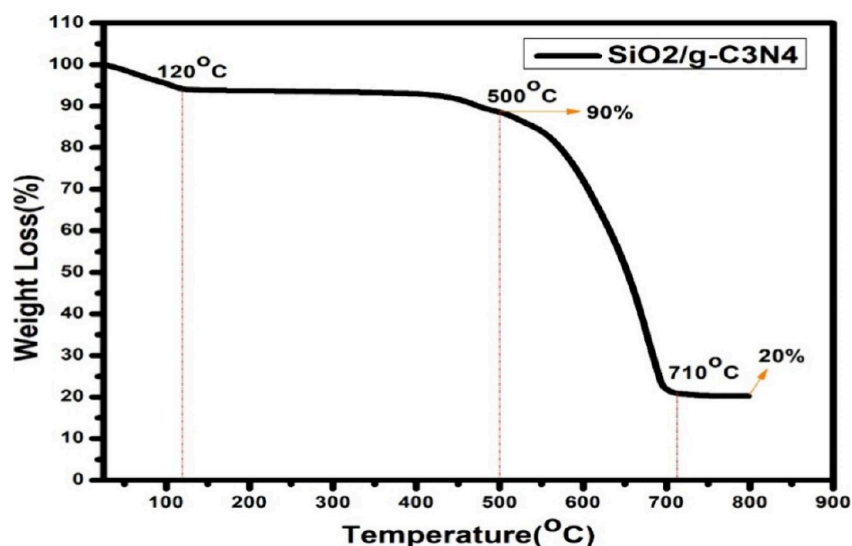


Figure 4. TGA curve of $\text{SiO}_2/\text{g-C}_3\text{N}_4$.

Table 2. Properties of the Developed Base Drilling Fluids with and without Nanomaterials^a

Properties	base mud		0.5 lb/bbl $\text{SiO}_2/\text{g-C}_3\text{N}_4$		1 lb/bbl $\text{SiO}_2/\text{g-C}_3\text{N}_4$		1.5 lb/bbl $\text{SiO}_2/\text{g-C}_3\text{N}_4$	
	BHR	AHR	BHR	AHR	BHR	AHR	BHR	AHR
M.W	1.20	1.20	1.20	1.20	1.20	1.20	1.20	1.20
viscometer dial readings								
600 rpm	52	26	65	70	68	72	73	78
300 rpm	36	19	48	54	51	57	54	62
200 rpm	30	16	41	48	42	50	44	53
100 rpm	22	12	31	36	32	39	35	42
6 rpm	8	5	11	14	12	19	14	21
3 rpm	6	4	6	11	9	16	10	18
PV (cP)	16	7	17	16	17	15	19	16
AV (Cp)	26	13	32.5	35	34	36	36.5	39
YP (lb/100 ft ²)	20	12	31	38	34	42	35	46
gel' (lb/100 ft ²)	7	5	10	12	11	14	12	14
gel'' (lb/100 ft ²)	10	8	22	21	25	22	26	24
API FL (mL)	6	12.5	5.5	6.5	5.5	6	5.2	5.6
cake (mm)	1.0	2.5	0.5	0.5	0.5	1	0.5	1
pH	8.0	8.0	8.5	8.0	8.0	8.0	8.0	8.0

^aAHR: after hot rolling; BHR: before hot rolling; API FL: API fluid loss.

the rheological characteristics of synthesized drilling fluid formulations, yield point, and plastic viscosity and gelling properties.

The rheological properties of drilling fluid improved with increasing nanomaterial concentrations according to experiments. With increasing $\text{SiO}_2/\text{g-C}_3\text{N}_4$ concentration, yield point (YP) and apparent viscosity (AV) rose dramatically. The improved hydrogen bonding is due to the synergistic actions of the nanomaterial and xanthan gum polymer. Because drilling fluid is exposed to varied shear rates inside the wellbore throughout the drilling operation,^{51,52} a reasonable range of apparent viscosity (AV) is necessary for the cutting flow. At higher concentrations of the nanomaterial, a slight increase in plastic viscosity was observed. To produce an alkaline environment, the pH of the drilling fluid compositions was kept between 8.0 and 8.5 using potassium hydroxide. The hot rolling conditions of the drilling fluid are as follows: temperature, 225 °F; time, 16 h.

The effectiveness of cleaning holes is influenced by the fluid viscosity and the yield point. As shown in Figure 5 and Table

2, the addition of 0.5, 1.0, and 1.5 lb/bbl $\text{SiO}_2-\text{C}_3\text{N}_4$ NPs significantly increase the viscosity of water-based drilling fluids. As part of its role as a yield point enhancer, the xanthan gum polymer also frequently increases the fluid viscosity. However, a nanocomposite's chain joiner sites aid in postincreasing the stable viscosity.

The gel strength of the drilling fluid, which is an important component, determines its ability to keep the drill cuttings suspended. According to experimental results, the $\text{SiO}_2/\text{g-C}_3\text{N}_4$ NPs also depicted an acceptable gel strength at both 10 s and 10 min, as shown in Table 2 and Figure 5c. The water-based drilling fluid's 10 s gel strength was 7 lb/100 ft² before being enhanced to 10 lb/100 ft² by the addition of 0.5 lb/bbl of $\text{SiO}_2/\text{g-C}_3\text{N}_4$ nanoparticles. After hot rolling, it was observed that the gel strength of base mud decreased to 5 lb/100 ft², but the gel strengths of the fluid treated with 0.5, 1, and 1.5 lb/bbl $\text{SiO}_2/\text{g-C}_3\text{N}_4$ nanoparticles significantly improved to 12, 14, and 14 lb/100 ft², respectively. This enhancement may be due to the nanoparticles' capacity to serve as chain joiner sites between the polymer matrices

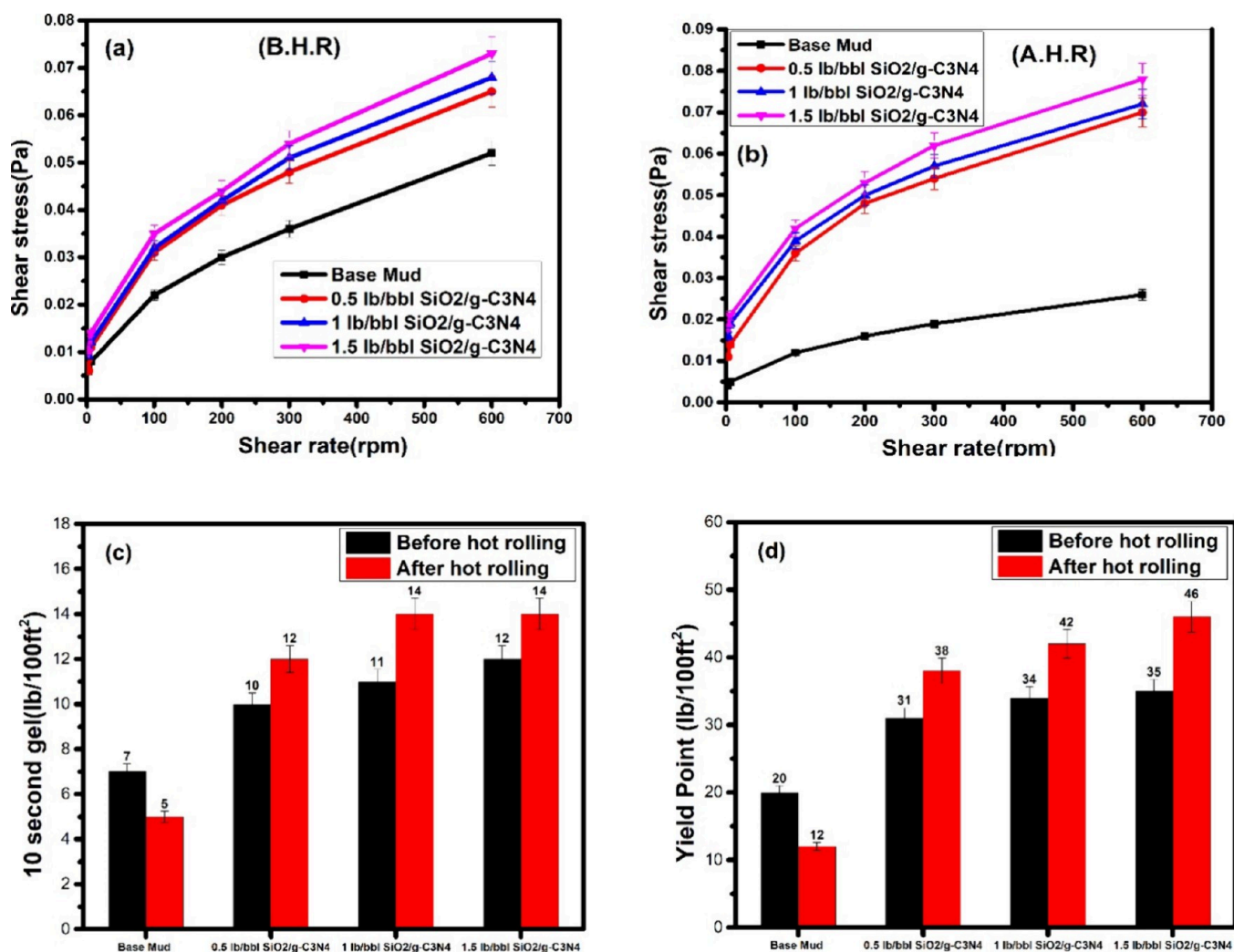


Figure 5. Drilling fluids shear rate and shear stress with different concentrations of nanomaterial and base fluid (a) before hot rolling (BHR); (b) after hot rolling. (c) Gel strength of drilling fluids BHR and AHR. (d) Yield point (YP) of drilling fluids BHR and AHR.

(Xanthan gum) and aid the gelation behavior of the nanocomposite drilling fluid. The results demonstrate that synthesized nanohybrid considerably influences the rheological characteristics of the generated drilling fluid system more than xanthan gum polymer and silicon oxide nanoparticles do separately.

3.5.1. Plastic Viscosity (PV). The viscosity of mud is described by a Bingham model component termed plastic viscosity (PV), which may be extended to an infinite shear rate using the Bingham model's mathematics.⁵³ Drillers often avoid utilizing high PV drilling fluids for drilling operations since they are difficult to pump. However, in order to increase hydrostatic pressure, which is directly connected to mud viscosity, a drilling fluid must be of sufficient density. Reduced mud viscosity leads to decreased mud density and, it appears, lower hydrostatic pressure, which is not always desired. As a result, in order to conduct safe drilling operations, an optimal value of PV should be established by taking into account all operational factors and the necessary mud properties.⁵⁴ Before hot rolling (BHR) and after hot rolling (AHR), the PV of base mud was measured to be 16 and 7 cP, respectively.

According to Table 2, adding SiO₂/g-C₃N₄ NPs often led to an increase in PV of the base mud. The value of PV for each kind of NPs at different concentrations (from 0.5 to 1.5 lb/

bbbl) was, however, nearly identical. The base mud did not sustain their PV value during hot rolling, as evidenced by data that showed that the PV value of the base mud reduced after hot rolling by almost half. The PV values of the 0.5, 1, and 1.5 lb/bbl SiO₂/g-C₃N₄ NPs were 17, 17, and 19 cP before hot rolling and 16, 15, and 16 cP after hot rolling, respectively. The results above demonstrate that the PV value of NPs treated mud systems did not decrease. This can be attributed to the fact that SiO₂/g-C₃N₄ NPs retain their structural integrity and bentonite–bentonite coupling capabilities. SiO₂/g-C₃N₄ NPs can improve the flow characteristics of base mud by a number of mechanisms, the majority of which are dependent on the mud system's continuous phase and the SiO₂/g-C₃N₄ NPs features. SiO₂/g-C₃N₄ NPs frequently enhance the apparent viscosity of base mud, the continuous phase of drilling fluids. It is well-known that the viscosity of nanofluids is much higher than that of regular dispersions for a given volume concentration of dispersed particles; after NPs are dispersed in the fluid, this friction may increase, increasing the viscosity of the nanofluid.^{55,56} Essential physical properties that influence how drilling fluid rheological characteristics change include the NPs density, structure, and heat capacity. The NPs and base mud may be linked or bound together directly or

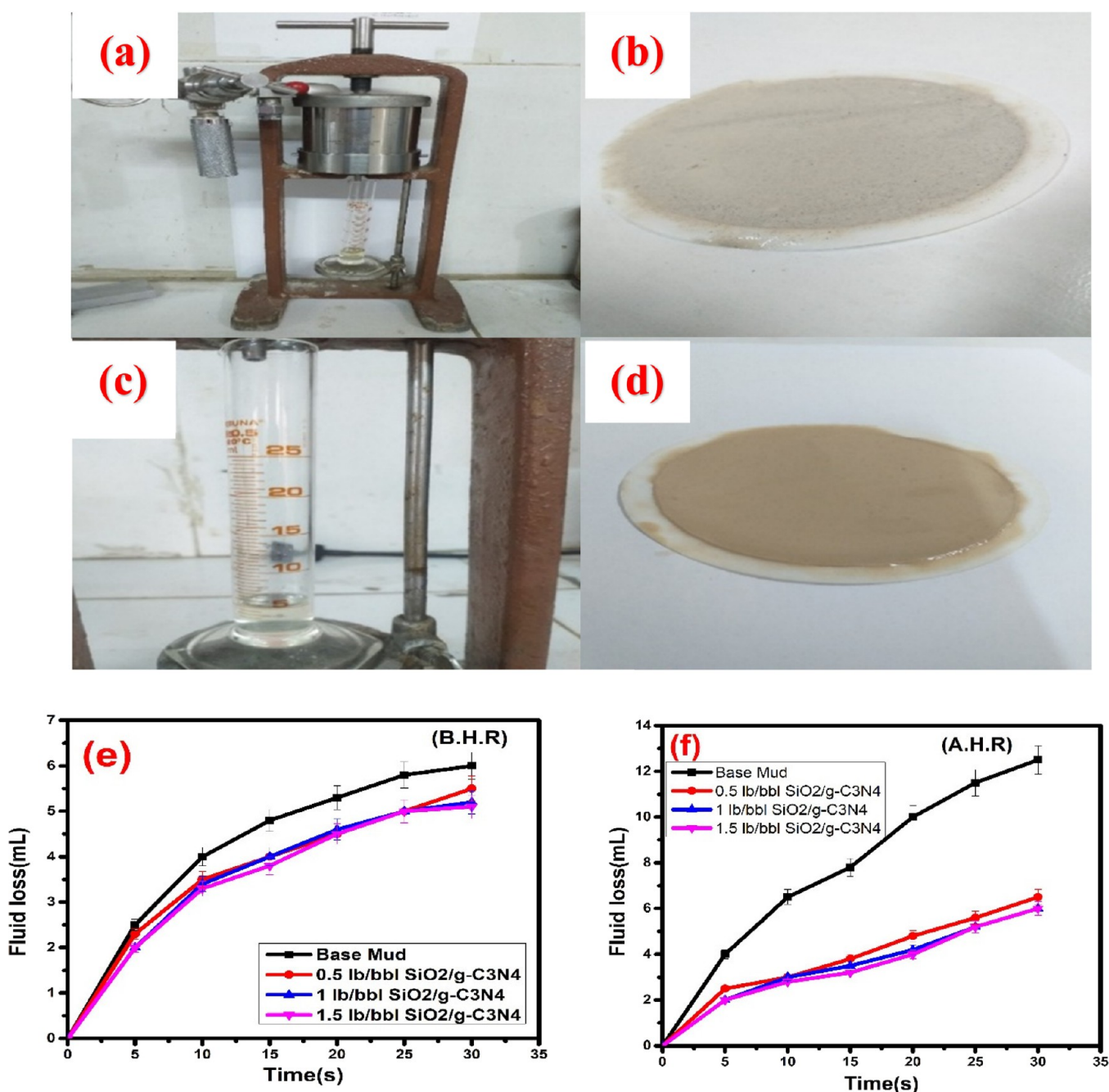


Figure 6. (a) OFITE 141–00-C API filter press used to check fluid loss. (b) OFITE filter paper obtained after API filter press of 0.5 SiO₂/g-C₃N₄. (c) Corresponding fluid loss of 0.5 SiO₂/g-C₃N₄ in measuring cylinder. (d) OFITE filter paper obtained after API filter press of base fluid. (e) Comparative fluid loss of different formulations within different time periods BHR and (f) AHR.

through certain chemical interactions in order to increase the PV of the base mud.²⁰

3.5.2. Gel Strength. The ability of a drilling fluid to suspend drilling fluid particles depends on a number of essential properties, including gel strength.⁵⁷ The gel strength is used to determine the electrochemical forces present in the fluid under static conditions. Figure 5c shows the impact of SiO₂/g-C₃N₄ NPs on gel strength at different concentrations for 10 s and 10 min, respectively. The gel strength values for 10 s and 10 min were 7 and 10 lb/100 ft² respectively, which correspond to the first evaluation of base mud gel strength. According to Figure 5c, adding 0.5, 1, and 1.5 lb/bbl SiO₂/g-C₃N₄ NPs increased the gel strength of base mud to 10, 11, and 12 lb/100 ft² for 10

s tests and 22, 25, and 26 lb/100 ft² for 10 min tests, respectively. Additionally, it can be noted in the findings that NPs slightly enhanced the gel strength (10 s, 10 min) after hot rolling and decreased the gel strength of the base mud (see Figure 5c). High gel strength is also necessary to prevent a number of serious drilling issues.⁵⁸ The gelling characteristics of 0.5, 1, and 1.5 lb/bbl SiO₂/g-C₃N₄ NP concentrations are therefore shown to be superior to base mud.

3.5.3. Yield Point (YP). The key factor affecting fluid flow in the reverse direction is the yield point (YP). The capacity of drilling fluid to remove drilling cuttings from downhole and transport them to the surface is often accomplished via the YP characteristic.⁵⁹ Electrical ions in the vicinity of the active

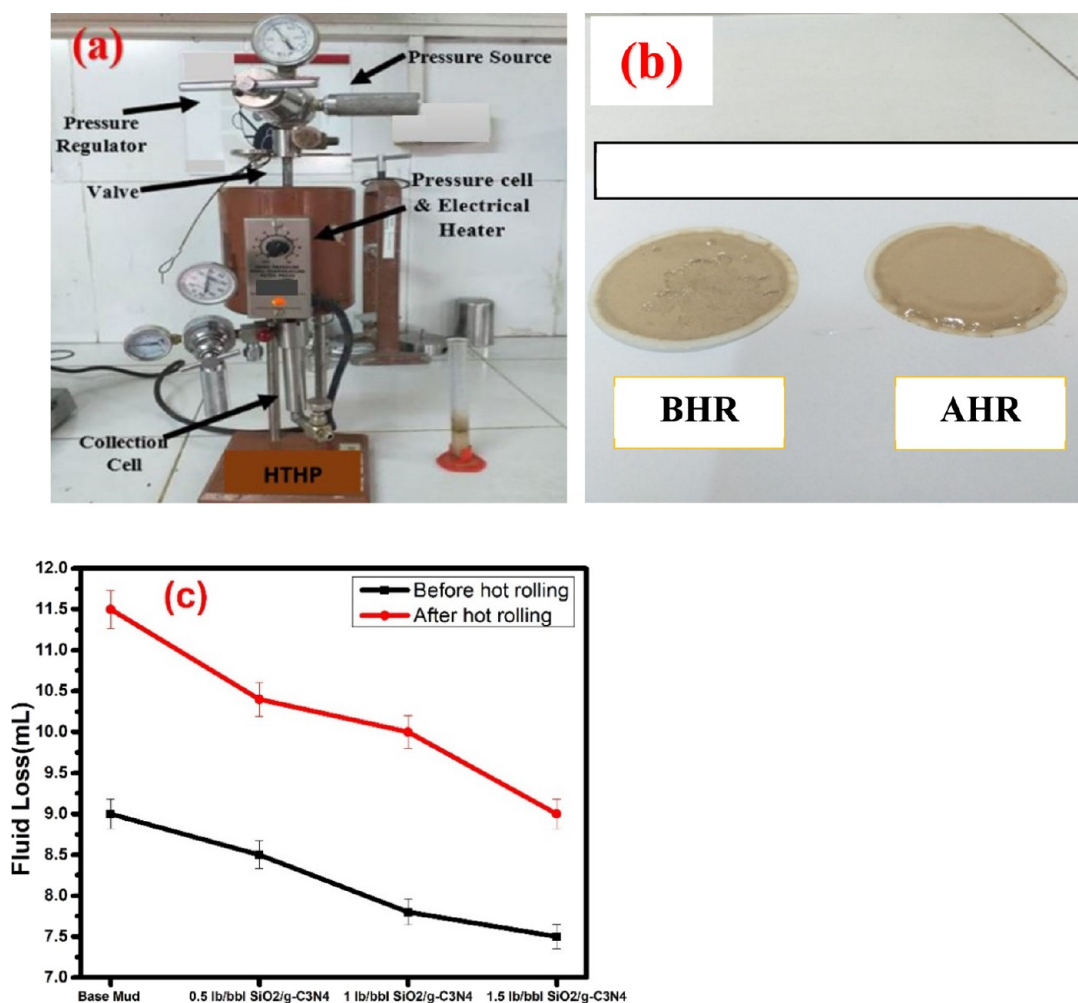


Figure 7. (a) OFITE high-pressure and high-temperature (HPHT) assembly. (b) OFITE filter obtained BHR and AHR of 0.5 ppb SiO₂/g-C₃N₄. (c) Bar chart to comparisons of HPHT fluid loss of different formulations.

chemical cause this parameter, which is introduced into a fluid via electrostatic forces. The electrical charges that are present on the surfaces of the interacting particles generate these electrochemical forces.⁵⁷ In particular, increasing the YP value enables drill cuttings to accelerate and carry faster toward the ground surface.⁶⁰ The YP needs to be high enough to initiate mud flow while still being low enough to prevent excessive pump pressure.⁶¹ Base mud YP was calculated to be 20 and 12 lb/100 ft² BHR and AHR, respectively. Figure 5d illustrates how SiO₂/g-C₃N₄ NPs affect the YP of based mud. When SiO₂/g-C₃N₄ NPs are present in varied quantities, the YP of base mud exhibits varying performances. At all tested concentrations, there is an increasing trend in the YP of the SiO₂/g-C₃N₄ NPs WBDF. For 1 lb/bbl SiO₂/g-C₃N₄ NPs, the highest yield point was 34 lb/100 ft² BHR and 42 lb/100 ft² AHR, respectively. The similar trend was seen in 0.5 lb/bbl SiO₂/g-C₃N₄ NP maximum yield point values of 31 lb/100 ft² and 38 lb/100 ft² BHR and AHR, respectively. As the concentration of NPs further increased to 1.5 lb/bbl SiO₂/g-C₃N₄, the yield point further increased to 35 lb/100 ft² and 46 lb/100 ft² BHR and AHR, respectively. The yield point value is enhanced by increasing concentrations. According to previous research, SiO₂/g-C₃N₄ NPs with larger surface area per volume may interact more with the matrix and the surrounding water-based drilling mud.⁶² Due to the particle bridging effect

created by the interaction of polar functional groups such as -OH, etc., situated in favorable locations to work with appealing interacting layers for having a high attraction to water.

3.5.4. Filtrate Loss. The mud cake thickness and fluid loss volume are the two important parameters that are measured in this type of experiment. The substantial amount of fluid loss volume is a damaging aspect for drilling fluids since it may lead to many problems, such as formation damage and instability of wellbore.^{46,63} The resulting pressure is effectively directed toward the formation at any point along the wellbore. This is because of the ongoing overbalance used to stop kicks from the formation. Mud is forced into the structure by this pressure. The fluid penetrates further into the formation, while the solid portion of the mud creates a thin plaster around the wellbore. If this filtrate loss occurs in shale, it may cause clay to swell. All of these result in increased complexity and deteriorated shale formation integrity in the first instance. A comparison of the fluid loss behavior of base mud and at different NPs concentrations is shown in Figure 6e,f. After 30 min, the base mud had 6 and 12.5 mL of fluid loss BHR and AHR, respectively. The fluid loss volume was 5.5 and 6.5 mL when 0.5 lb/bbl of SiO₂/g-C₃N₄ NPs were added to the base mud BHR and AHR, and it slightly reduced to 5.5 and 5.2 mL at 1 and 1.5 lb/bbl SiO₂/g-C₃N₄ NPs, respectively. The findings

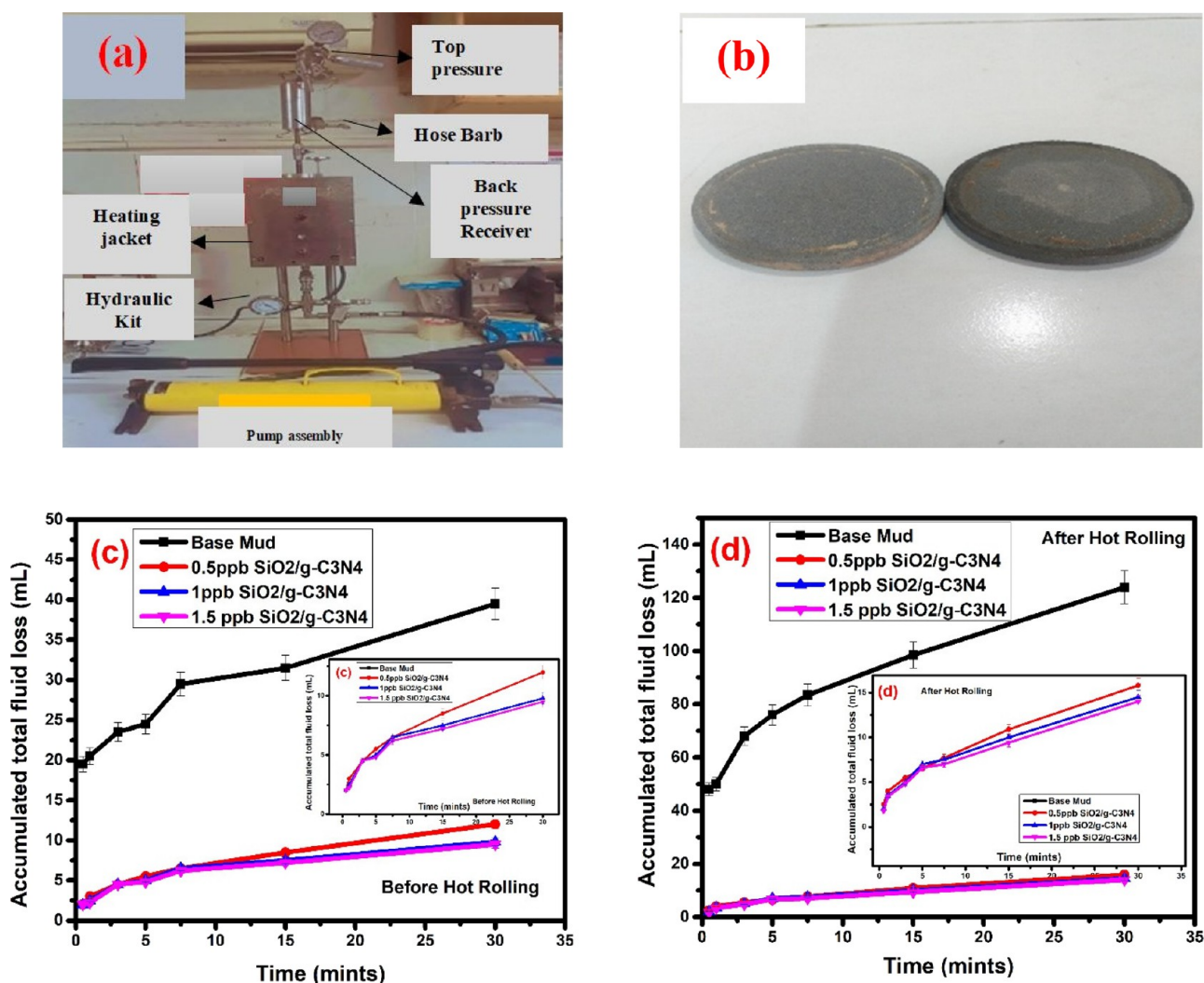


Figure 8. (a) OFTITE 171–85 permeability plugging tester apparatus. (b) 40 μm ceramic discs used in PPT. Accumulated total fluid loss of different formulations: (c) BHR; (d) AHR.

demonstrate that SiO₂/g-C₃N₄ NPs might be a potential addition to lower base mud fluid loss, particularly at concentrations between 0.5 and 1.5 lb/bbl. SiO₂/g-C₃N₄ NPs, which significantly decrease the base mud fluid loss (5.5 mL) at concentrations of 1.5 lb/bbl. After hot rolling, the base mud loses a significant amount of fluid because the polymeric materials (Polyanionic Cellulose, Modified Starch) used in the formulation lose their properties. However, NPs mud had nearly the same fluid loss in both BHR and AHR because NPs do not lose their properties and maintain structure and shape after hot rolling. Actually, when SiO₂/g-C₃N₄ NPs concentrations increased, the number of nanoparticles in the drilling fluid system increased, resulting in a drop in the mud cake thickness, which blocked extremely small holes and microscopic cavities in mud cake surfaces. As a result, the volume of mud filtration is reduced.

3.5.5. High Pressure and High Temperature. The filtration characteristics of the drilling fluid samples were evaluated by using the HPHT filtration test at 225 °F and 500 psi differential pressure, respectively. The filtrate loss and mud cake were measured after the test had run for 30 min. Figure 7 depicts a comparison of the efficacy of several drilling fluids under extreme pressure and heat. According to Figure 7,

filtration loss at HPHT up to 225 °F for the base mud showed considerable fluid loss as compared to SiO₂/g-C₃N₄ NPs mud performing better. At HPHT conditions, the base muds usually had a greater filtrate loss until a temperature of 225 °F. The filtrate loss from the base mud was higher than the filtrate loss from the muds containing SiO₂/g-C₃N₄ NPs at 225 °F.

Figure 7a depicts the HPHT apparatus used for this test, and Figure 7b depicts the mud cake that resulted from the test, with a thickness of 1 mm for 0.5 lb/bbl SiO₂/g-C₃N₄ NPs BHR and AHR. This mud cake has a smooth surface and is very thick. The cumulative fluid loss is shown in Figure 7c, and it is obvious from the graph that as the concentration of nanomaterials increased the fluid loss decreased, reaching minimums of 7.5 and 9.2 mL of BHR and AHR for 1.5 lb/bbl nanomaterial. This was due to the fact that polymers are temperature-sensitive, and under HPHT conditions, they breakdown, increasing fluid loss and impairing the ability to move cuttings upward.^{64,65} As compared to the base mud sample, SiO₂/g-C₃N₄ NPs outperformed in terms of filtrate loss volume. The performance of SiO₂/g-C₃N₄ NPs was caused by the edge-to-edge (positive edge bentonite–negative face bentonite) and face-to-face (modified silica and bentonite) electrostatic attraction. This arrangement traps silica in the

spaces between the clay granules, resulting in heterocoagulated formation cluster.^{66,67} The fluid within the formation is held and retained by this created structure, which lowers the volume loss of the filtrate. Daswani and Van Herk said that when two particles with different features, such as chemical composition, size, and charge, combine, clusters develop, which leads to the production of a gel-like structure known as heterocoagulation.⁶⁸

3.5.6. Permeability Plugging Test (PPT). A permeability plugging tester (PPT), which is a modification of the common HTHP filter press, is a device used to evaluate a drilling fluid's potential to plug pores in a ceramic disc. Drilling fluid was prepared and then placed in a PPT cell. A pump on the bottom side of the cell delivers the appropriate amount of pressure as it forces drilling through a ceramic disc that is set up on the top side of the cell. After 0.5, 1, 3, 5, 7.5, 15, and 30 min, the filtrate was collected in a receiver. The filter media is a ceramic disc, and the filtration area is 3.5 in², which is twice as small as API filtration. The experiments were run at a temperature of 225 °F and a differential pressure of 1000 psi, and the pore size of the employed ceramic discs was 40 μm. Equation 4 must be multiplied by 2 to account for the API filtration's twice as big filtration surface, while eq 5 may be used to determine the spurt loss.⁶⁹

$$\text{PPT filtrate volume} = 2 \times V_{30} \quad (4)$$

$$\text{spurt loss} = 4 \times V_{7.5} - 2 \times V_{30} \quad (5)$$

where V_{30} is the filtrate volume collected after 30 min in mL and $V_{7.5}$ is the filtrate volume collected after 7.5 min in mL. Spurt loss is defined as fluid volume collected before establishment of mud cake in mL.

Filtration through the ceramic disc, which has a pore size of 40 μm, resulted in a significant decrease in filtration volume after 30 min for tested nanomaterials drilling fluids containing 0.5, 1, and 1.5 lb/bbl SiO₂/g-C₃N₄ NPs (24, 19.6, and 19 mL, respectively) when compared to values measured with base drilling fluid (79 mL) for BHR. Using the spurt loss values, the quantity of fluid lost before developing the drilling fluid cake was greatly reduced for tested NP-containing drilling fluids as shown in Table 3. Because the tested disc has varying hole diameters, it is proven that NPs better plugged the disc pores

Table 3. PPT Results of Different Formulations with Ceramic Disc of a Pore Size of 40 μm

drilling fluids	base mud		0.5 lb/bbl SiO ₂ /g-C ₃ N ₄		1 lb/bbl SiO ₂ /g-C ₃ N ₄		1.5 lb/bbl SiO ₂ /g-C ₃ N ₄	
	BHR	AHR	BHR	AHR	BHR	AHR	BHR	AHR
$V_{0.5}$, mL	19.5	48	2	2.5	2	2	2	1.8
V_1 , mL	20.5	50	3	4	2.5	3.5	2.2	3.4
V_3 , mL	23.5	68	4.5	5.5	4.5	5	4.5	4.8
V_5 , mL	24.5	76	5.5	6.5	5	7	4.8	6.6
$V_{7.5}$, mL	29.5	83.5	6.5	8.5	6.5	7.5	6.2	7.2
V_{15} , mL	31.5	98.5	8.5	10.9	7.5	10	7.2	9.4
V_{30} , mL	39.5	124	12	15.8	9.8	14.5	9.5	14
PPT filtrate volume, mL	79	248	24	31.6	19.6	29	19	28
spurt loss, mL	39	86	2	2.4	6.4	1	5.8	0.8

than base mud passed through the disc before producing the drilling fluid cake. As 0.5, 1, and 1.5 lb/bbl SiO₂/g-C₃N₄ NPs are added to the drilling fluid, the invasion rate into the 40 μm disc is reduced by 69.6, 75.1, and 76%, respectively, as compared to the base drilling mud. AHR nanoparticles with 0.5, 1, and 1.5 lb/bbl SiO₂/g-C₃N₄ decreased the invasion rate by 87.2, 88.3, and 88.7%, respectively, which shows much more improvement than nonfunctionalized and high- and low-carboxyl-functionalized SiO₂, which reduced the filtration by 13, 33, and 36%.⁷⁰

According to the data, AHR, base mud has a total loss after 30 min, indicating that polymeric materials lose their characteristics, and NPs are more effective. AHR results indicate that the NPs considerably plugged the pores and reduced fluid penetration.

4. CONCLUSIONS

In this work, SiO₂/g-C₃N₄ NPs mud with different concentrations including 0.5, 1, and 1.5 lb/bbl NPs were produced. It was determined through this experimental research that SiO₂/g-C₃N₄ is effective for enhancing WBM fluids. A g-C₃N₄ was grafted onto the surface of silica NPs to modify them. The results show that this was an effective method for lowering silica NPs aggregation, leading to better mud system properties. It will be desirable to utilize g-C₃N₄ modified silica NPs in drilling mud systems when silica is in a good, disseminated form since stability was important in the experimental study. The nanoparticles were subsequently dispersed in water using the well-known two-step techniques to make nanofluids. The generated nanofluids were then added to the drilling mud to improve its filtration and rheological properties. The following are the conclusions of the experiments conducted for this study:

1. The addition of nanoparticles to base mud improves the rheological characteristics of the drilling fluid. This improvement is proportional to the size and concentration of nanoparticles. For 1 and 1.5 lb/bbl SiO₂/g-C₃N₄ NPs, the highest yield points were 34 and 35 lb/100 ft² BHR and 42 and 46 lb/100 ft² AHR, respectively. A similar trend was seen in 0.5 lb/bbl SiO₂/g-C₃N₄ NPs with maximum yield point values of 31 and 38 lb/100 ft² BHR and AHR, respectively.
2. Nanoparticles treated drilling fluid has substantially lower fluid loss in PPT before and after hot rolling than base mud. As 0.5, 1, and 1.5 lb/bbl SiO₂/g-C₃N₄ NPs are added to the drilling fluid, the fluid loss reduced by 69.6, 75.1, and 76%, respectively, as compared to the base drilling mud. AHR nanoparticles with 0.5, 1, and 1.5 lb/bbl SiO₂/g-C₃N₄ NPs decreased the fluid loss by 87.2, 88.3, and 88.7% respectively.
3. Adding nanoparticles to drilling fluids successfully increases their thermal stability.
4. We understand that the hybrid SiO₂/g-C₃N₄ has been investigated for the first time in this study to enhance the properties of the water-based drilling fluids.

AUTHOR INFORMATION

Corresponding Author

Erum Pervaiz – Department of Chemical Engineering, School of Chemical and Materials Engineering (SCME), National University of Sciences & Technology (NUST), Islamabad

44000, Pakistan; orcid.org/0000-0003-1498-2167;
Email: erum.pervaiz@scme.nust.edu.pk

Authors

Anwar Ahmed – Department of Chemical Engineering, School of Chemical and Materials Engineering (SCME), National University of Sciences & Technology (NUST), Islamabad 44000, Pakistan

Uzair Abdullah – Department of Chemical Engineering, School of Chemical and Materials Engineering (SCME), National University of Sciences & Technology (NUST), Islamabad 44000, Pakistan

Tayyaba Noor – Department of Chemical Engineering, School of Chemical and Materials Engineering (SCME), National University of Sciences & Technology (NUST), Islamabad 44000, Pakistan

Complete contact information is available at:

<https://pubs.acs.org/10.1021/acsomega.3c08766>

Notes

The authors declare no competing financial interest.

†Anwar Ahmed, Dr. Erum Pervaiz, Uzair Abdullah, and Dr. Tayyaba Noor

ACKNOWLEDGMENTS

Authors would like to acknowledge SCME, NUST for support in this study.

REFERENCES

- (1) Ma, J.; et al. Experimental study on the polymer/graphene oxide composite as a fluid loss agent for water-based drilling fluids. *ACS omega* **2021**, *6* (14), 9750–9763.
- (2) Bardhan, A. et al. Performance Evaluation of Novel Silane Coated Nanoparticles as an Additive for High-Performance Drilling Fluid Applications. in *International Petroleum Technology Conference*. 2023. OnePetro DOI: DOI: 10.2523/IPTC-22878-MS.
- (3) Al-Yasiri, M. S. W.T.J.A.J.o.N.r. Al-Sallami, and applications, How the drilling fluids can be made more efficient by using nanomaterials. *Am. J. Nano Res. Appl.* **2015**, *3* (3), 41–45.
- (4) Zhu, W.; Zheng, X.J.A.o. Effective modified xanthan gum fluid loss agent for high-temperature water-based drilling fluid and the filtration control mechanism. *ACS omega* **2021**, *6* (37), 23788–23801.
- (5) Srivastava, V.; et al. Application of manganese oxide nanoparticles synthesized via green route for improved performance of water-based drilling fluids. *Applied Nanoscience* **2021**, *11*, 2247–2260.
- (6) Barry, M. M.; et al. Fluid filtration and rheological properties of nanoparticle additive and intercalated clay hybrid bentonite drilling fluids. *J. Pet. Sci. Eng.* **2015**, *127*, 338–346.
- (7) Contreras, O. et al. Application of in-house prepared nanoparticles as filtration control additive to reduce formation damage. in *SPE International Symposium and Exhibition on Formation Damage Control*. 2014. OnePetro DOI: DOI: 10.2118/168116-MS.
- (8) Li, H., et al., Improving the anti-collapse performance of water-based drilling fluids of Xinjiang Oilfield using hydrophobically modified silica nanoparticles with cationic surfactants. *Pet. Sci.*, **2023**, *20*(3) DOI: 1768.
- (9) Perween, S.; et al. Effect of zinc titanate nanoparticles on rheological and filtration properties of water based drilling fluids. *Journal of Petroleum Science & Engineering* **2018**, *170*, 844–857.
- (10) Archer, R., Geothermal energy, in *Future Energy*. 2020, Elsevier. p 431–445.
- (11) Vollmar, D.; Wittig, V.; Bracke, R.J.I.G.A.H. *Geothermal Drilling Best Practices: The Geothermal translation of conventional drilling recommendations-main potential challenges*. International Geothermal Association, 2013.
- (12) Ni, X.; et al. Synthesis of superhydrophobic nanofluids as shale inhibitor and study of the inhibition mechanism. *Appl. Surf. Sci.* **2019**, *484*, 957–965.
- (13) Yue, Y.; et al. Improving wellbore stability of shale by adjusting its wettability. *J. Pet. Sci. Eng.* **2018**, *161*, 692–702.
- (14) Ibrahim, M. A.; Saleh, T.A.J.C.r. Partially aminated acrylic acid grafted activated carbon as inexpensive shale hydration inhibitor. *Carbohydr. Res.* **2020**, *491*, No. 107960.
- (15) Rivet, S. M. *Coreflooding oil displacements with low salinity brine*. 2009, The university of Texas austin.
- (16) Zamora-Ledezma, C., et al., Nanofluid formulations based on two-dimensional nanoparticles, their performance, and potential application as water-based drilling fluids. 2022. *7*(24): p 20457–20476.
- (17) Sheshdeh, M. J. A review study of wettability alteration methods with regard to nano-materials application. in *SPE Bergen One Day Seminar*. 2015. OnePetro DOI: DOI: 10.2118/173884-MS.
- (18) Al-Ansari, S.; et al. Wettability alteration of oil-wet carbonate by silica nanofluid. *J. Colloid Interface Sci.* **2016**, *461*, 435–442.
- (19) Mao, H.; et al. Hydrophobic associated polymer based silica nanoparticles composite with core-shell structure as a filtrate reducer for drilling fluid at ultra-high temperature. *Geoenergy Sci. Eng.* **2015**, *129*, 1–14.
- (20) Kang, Y.; et al. Strengthening shale wellbore with silica nanoparticles drilling fluid. *Pet. Sci.* **2016**, *2* (2), 189–195.
- (21) Misbah, B.; et al. Friction reduction of Al₂O₃, SiO₂, and TiO₂ nanoparticles added to non-Newtonian water based mud in a rotating medium. *J. Pet. Sci. Eng.* **2022**, *217*, No. 110927.
- (22) Pu, L.; et al. Enhanced stability of low oil-to-water ratio water-in-oil emulsions (oil-based drilling fluids): Synergistic effect of nano-SiO₂ and emulsifiers. *J. Pet. Sci. Eng.* **2022**, *219*, No. 111053.
- (23) Shen, Y.; et al. Nano-SiO₂ Grafted with Temperature-Sensitive Polymer as Plugging Agent for Water-Based Drilling Fluids. *Arabian J. Sci. Eng.* **2022**, 1–11.
- (24) Bardhan, A.; et al. Utilization of mesoporous nano-silica as high-temperature water-based drilling fluids additive: Insights into the fluid loss reduction and shale stabilization potential. *Geoenergy Sci. Eng.* **2024**, *232*, No. 212436.
- (25) Li, Y.; et al. Application of hybrid silicate as a film-forming agent in high-temperature water-based drilling fluids. *ACS omega* **2021**, *6* (31), 20577–20589.
- (26) Saleh, T. A.; et al. Synthesis of novel hydrophobic nanocomposite-modified silica as efficient shale inhibitor in fuel industry. *Surfaces and Interfaces* **2023**, *38*, No. 102837.
- (27) Rana, A.; et al. Advances in Carbon nanostructures and nanocellulose as additives for efficient drilling fluids: Trends and future perspective—A review. *Energy Fuels* **2021**, *35* (9), 7319–7339.
- (28) Ahmed, A.; Pervaiz, E.; Noor, T. J. C. Applications of Emerging Nanomaterials in Drilling Fluids. *ChemistrySelect* **2022**, *7* (43), e202202383.
- (29) Ibrahim, M. A.; et al. A review on the effect of nanoparticle in drilling fluid on filtration and formation damage. *J. Pet. Sci. Eng.* **2022**, *217*, No. 110922.
- (30) Razali, S. Z.; et al. Effects of morphology and graphitization of carbon nanomaterials on the rheology, emulsion stability, and filtration control ability of drilling fluids. *J. Mater. Res. Technol.* **2022**, *21*, 2891–2905.
- (31) Ajdary, R.; et al. Plant nanomaterials and inspiration from nature: water interactions and hierarchically structured hydrogels. *Adv. Mater.* **2021**, *33* (28), 2001085.
- (32) Abdullah, A. H.; et al. A comprehensive review of nanoparticles in water-based drilling fluids on wellbore stability. *Chemosphere* **2022**, *308*, No. 136274.
- (33) Ahmed, A.; et al. Enhancing the thermal, mechanical and swelling properties of PVA/starch nanocomposite membranes incorporating g-C₃N₄. *J. Polym. Environ.* **2020**, *28* (1), 100–115.
- (34) Wang, B.; et al. α -Fe₂O₃ nanoparticles/porous g-C₃N₄ hybrids synthesized by calcinations of Fe-based MOF/melamine

mixtures for boosting visible-light photocatalytic tetracycline degradation. *ChemistrySelect* **2020**, *5* (11), 3303–3311.

(35) Xu, J.; et al. A facile cooling strategy for the preparation of silica nanoparticles with rough surface utilizing a modified Stöber system. *Colloids Surf., A* **2021**, *625*, No. 126845.

(36) Sivolapov, P.; Myronyuk, O.; Baklan, D.J.I.C.C. Synthesis of Stober silica nanoparticles in solvent environments with different Hansen solubility parameters. *Inorg. Chem. Commun.* **2022**, *143*, No. 109769.

(37) Bogush, G.; Tracy, M.; Zukoski Iv, C.J.J.o.n.-c.s. Preparation of monodisperse silica particles: control of size and mass fraction. *J. Non-Cryst. Solids* **1988**, *104* (1), 95–106.

(38) Arain, A. H.; et al. Development and performance evaluation of castor oil based biodiesel as an eco-friendly ester-based drilling fluid. *Pet. Sci. Technol.* **2022**, *41* (19), 1–21.

(39) Yao, Q.; et al. Ultrafine Ru nanoparticles embedded in SiO₂ nanospheres: highly efficient catalysts for hydrolytic dehydrogenation of ammonia borane. *J. Power Sources* **2014**, *257*, 293–299.

(40) Nair, A.; et al. Prediction of size, precursor ratio and monodispersity of silica nanospheres through adaptive neuro-fuzzy inference system. *Chemical Physics Impact* **2022**, *4*, No. 100042.

(41) Wang, X.; et al. A metal-free polymeric photocatalyst for hydrogen production from water under visible light. *Nat. Mater.* **2009**, *8* (1), 76–80.

(42) Cao, K.; et al. Highly water-selective hybrid membrane by incorporating g-C₃N₄ nanosheets into polymer matrix. *J. Membr. Sci.* **2015**, *490*, 72–83.

(43) Mo, Z.; et al. Synthesis of gC 3 N 4 at different temperatures for superior visible/UV photocatalytic performance and photo-electrochemical sensing of MB solution. *RSC Adv.* **2015**, *5* (123), 101552–101562.

(44) Dong, F.; et al. Enhanced visible light photocatalytic activity and oxidation ability of porous graphene-like g-C₃N₄ nanosheets via thermal exfoliation. *Appl. Surf. Sci.* **2015**, *358*, 393–403.

(45) Kim, M.; Hwang, S.; Yu, J.-S.J.J.o.M.C. Novel ordered nanoporous graphitic C 3 N 4 as a support for Pt–Ru anode catalyst in direct methanol fuel cell. *J. Mater. Chem.* **2007**, *17* (17), 1656–1659.

(46) Narkbuakaew, T.; Sujaridworakun, P.J.T.i.C. *Synthesis of Tri-S-Triazine Based g-C₃N₄ Photocatalyst for Cationic Rhodamine B Degradation under Visible Light*. Springer, 2020. 63(11–14): p 1086–1096 DOI: [DOI: 10.1007/s11244-020-01375-z](https://doi.org/10.1007/s11244-020-01375-z).

(47) Liu, C.; et al. Pellet silica-based titanate adsorbents with high selectivity for strontium removal from synthetic radioactive solutions. *J. Sol-Gel Sci. Technol.* **2019**, *91*, 273–285.

(48) Kim, T. G.; et al. Synthesis of size controlled spherical silica nanoparticles via sol-gel process within hydrophilic solvent. *Korean Ceramic Society* **2017**, *54* (1), 49–54.

(49) Cao, S.; et al. Polymeric photocatalysts based on graphitic carbon nitride. *Adv. Mater.* **2015**, *27* (13), 2150–2176.

(50) Feng, P.; et al. The significance of dispersion of nano-SiO₂ on early age hydration of cement pastes. *Mater. Des.* **2020**, *186*, No. 108320.

(51) Abdo, J.; et al. ZnO–clay nanocomposites for enhance drilling at HTHP conditions. *Surf. Interface Anal.* **2014**, *46* (10–11), 970–974.

(52) Mohamed, A.; Salehi, S.; Ahmed, R. J. G. Significance and complications of drilling fluid rheology in geothermal drilling: A review. *Geothermics* **2021**, *93*, No. 102066.

(53) Güneysi, E.; et al. Rheological and fresh properties of self-compacting concretes containing coarse and fine recycled concrete aggregates. *Constr. Build. Mater.* **2016**, *113*, 622–630.

(54) Piroozian, A.; et al. Impact of drilling fluid viscosity, velocity and hole inclination on cuttings transport in horizontal and highly deviated wells. *J. Pet. Explor. Prod. Technol.* **2012**, *2*, 149–156.

(55) Rafati, R.; et al. Effect of nanoparticles on the modifications of drilling fluids properties: A review of recent advances. *J. Pet. Sci. Eng.* **2018**, *161*, 61–76.

(56) Sharma, A. K.; et al. Rheological behaviour of nanofluids: A review. *Renewable Sustainable Energy Rev.* **2016**, *53*, 779–791.

(57) Ramesh, K. T.; Ramesh, K. *Nanomaterials*. 2009: Springer.

(58) Ghosn, R.; et al. Silica nanoparticles for the stabilization of W/O emulsions at HTHP conditions for unconventional reserves drilling operations. *Oil Gas Sci. Technol. – Rev.* **2017**, *72* (4), 21.

(59) Busahmin, B.; et al. Review on hole cleaning for horizontal wells. *J. Eng. Appl. Sci.* **2017**, *12* (16), 4697–4708.

(60) Noah, A.; et al. Enhancement of yield point at high pressure high temperature wells by using polymer nanocomposites based on ZnO & CaCO₃ nanoparticles. *Egypt. J. Pet.* **2017**, *26* (1), 33–40.

(61) Agarwal, S. et al. Flow behavior of nanoparticle stabilized drilling fluids and effect of high temperature aging. in *AADE national technical conference and exhibition*. 2011.

(62) Quintero, L.; Cardenas, A.E.; Clark, D.E. *Nanofluids and methods of use for drilling and completion fluids*. 2014, Google Patents.

(63) Movahedi, H.; Jamshidi, S.; Hajipour, M.J.A.o., Hydrodynamic Analysis and Cake Erosion Properties of a Modified Water-Based Drilling Fluid by a Polyacrylamide/Silica Nanocomposite during Rotating-Disk Dynamic Filtration. 2022. 7(48): p 44223–44240.

(64) Kelessidis, V.; et al. Permeability, porosity and surface characteristics of filter cakes from water–bentonite suspensions. *Trans. Eng. Sci.* **2007**, *56*, 173–182.

(65) Adam, T. B., et al., Applied drilling engineering. *SPE* 1991. 2.

(66) Elochukwu, H.; et al. An approach to improve the cuttings carrying capacity of nanosilica based muds. *J. Pet. Sci. Eng.* **2017**, *152*, 309–316.

(67) Guan, O. S.; et al. A nano-particle based approach to improve filtration control of water based muds under high pressure high temperature conditions. *Pet. Sci.* **2020**, *6* (1), 43–52.

(68) Daswani, P.; Van Herk, A.J.E.o.P.N. Hetero-coagulation. *J. Colloid Interface Sci.* **2014**, *139* (1), 978–973.

(69) Manual, P.P.T.I.J.I.H. *TX, USA, Ver. 5.0; OFI Testing Equipment*. 2015.

(70) Ibrahim, M. A.; et al. The effect of surface properties of silicon dioxide nanoparticle in drilling fluid on return permeability. *Geoenergy Sci. Eng.* **2023**, *227*, No. 211867.